Available online at www.sciencedirect.com
ScienceDirect
Journal of Computational Physics 226 (2007) 571–585
JOURNAL OF COMPUTATIONAL PHYSICS
www.elsevier.com/locate/jcp

Equation Free Projective Integration: A multiscale method applied to a plasma ion acoustic wave

M.A. Shay [a,*], J.F. Drake [b], B. Dorland [b]

[a] Department of Physics and Astronomy, University of Delaware, Newark, DE 19716, United States
[b] Institute for Research in Electronics and Applied Physics, University of Maryland, College Park, MD 20742, United States

Received 4 June 2006; received in revised form 16 April 2007; accepted 20 April 2007
Available online 1 May 2007

Abstract

Multiscale problems such as magnetic reconnection and turbulence are notoriously hard to simulate because the physics of micro and macroscales are strongly linked. This study is the first application of a novel numerical scheme called Equation Free Projective Integration (EFPI) to a plasma system: we simulate the propagation and steepening of a 1D ion acoustic wave. In EFPI, the simulations act on two scales, an "inner" microscale and an "outer" coarse scale. The long timescale dynamic behavior of the system is determined by extrapolating forward estimates of the coarse scales obtained from short duration simulations of the microscale dynamics. There are no explicit closed-form equations governing the coarse scales, hence the name "Equation Free." In this study, a kinetic particle-in-cell code called P3D is used to simulate the microscale dynamics. We find excellent agreement between P3D and EFREE, the EFPI code. The differences which occur between the two are not due to numerical accuracy issues, but instead are caused by an incomplete representation of the system at coarse scales. More specifically, as the ion acoustic wave becomes a shock with Debye length scales, the assumptions of quasi-neutrality and maxwellian ions become invalid. Generalizing the "outer" coarse representation of the system to include non-maxwellian ions and Debye length structures should minimize the differences between P3D and EFREE. The largest EFREE run in this study showed a speedup of about 13 times over its P3D counterpart. Remarkably, the speedup of EFREE over P3D scales linearly with system size: the larger the simulation, the greater the speedup. The results indicate that EFPI is a potential candidate for simulating multiscale plasma problems.

Keywords: Plasma physics; Ion acoustic wave; Multiscale computations; Computer simulations; Multiscale physics; Projective integration; Equation Free Projective Integration; Full particle simulations

1. Introduction

Numerical simulations have allowed great leaps forward in our understanding of many physical systems. However, there is one class of problems, multiscale problems, that have defied brute force numerical methods.

* Corresponding author. Tel.: +1 302 831 2677; fax: +1 302 831 1637.
E-mail address: shay@physics.udel.edu (M.A. Shay).

0021-9991/$ - see front matter © 2007 Elsevier Inc. All rights reserved.
doi:10.1016/j.jcp.2007.04.016

Multiscale systems are those systems that exhibit behavior in which there is a direct linkage between the physics at very small lengthscales/fast timescales and the behavior at large lengthscales/slow timescales. In plasmas, two important multiscale problems are magnetic reconnection and turbulence. During magnetic reconnection, magnetic field lines are allowed to break and reform at extremely small length scales, releasing large amounts of magnetic energy in the form of plasma flows and heating. Reconnection can have a macroscopic effect, however, releasing energy during solar flares and causing the global convection patterns seen in the Earth's magnetosphere. In laboratory fusion plasmas, on the other hand, the properties of very small scale turbulence can determine the transport properties of the whole system. The nature of the transport ultimately determines if the experimental device can keep the plasma at high enough pressure to allow fusion to occur.

In this paper we apply a particular multiscale computational algorithm, called Equation Free Projective Integration (EFPI) to plasmas [1–5]. Other techniques are also being studied for application to multiscale problems [6–11].

The usual way of simulating systems that have disparate scales is to first derive a set of reduced equations valid at large scales and then solve that set of equations using a numerical algorithm. EFPI, on the other hand, relies on microscopic simulations which include all small scale physics instead of reduced equations. A numerical algorithm is then used to map those microscopic simulation results to coarse (macroscopic) scales and use them to evolve the global behavior of the system. The advantage of using microscopic simulations coupled with a numerical mapping algorithm is that it has the potential to implicitly account for the macroscopic effects of the microscale physics. There must be sufficient separation of scales, however, between the microscale physics and the macroscale physics in order for EFPI to be effective.

EFPI is a novel technique which needs to be studied carefully in order to evaluate its strengths and weaknesses and determine if it has the potential to allow multiscale plasma simulations not possible with conventional techniques. We emphasize that this technique is not guaranteed to succeed in modeling multiscale plasma, but if successful the payoff is large enough to justify the time spent studying it. A first step in this process is to apply EFPI to a straightforward plasma problem and compare it with trusted simulation results. In this paper, therefore, we simulate the propagation and steepening of a 1D ion acoustic wave using both a kinetic particle-in-cell (PIC) code as well as an EFPI code and compare the results. Note that the ion acoustic wave is not a multiscale problem, nor should one draw the conclusion that EFPI in its current state is more effective at simulating this wave than other more conventional kinetic plasma simulation techniques: Implicit moment kinetic PIC codes, for example, use approximations of the particle moments to estimate the future values of the fields which accelerate the particles [12–15]. Direct implicit kinetic PIC codes work directly with the particle equations of motion, but linearizes them to allow an estimate of their future values used in the implicit scheme [16–19]. ''Multiscale'' PIC codes use different step sizes for different spatial regions of the codes, depending on the relevant gradient scales in each region [20]. ''Multiscale'' PIC codes have been used to simulate the propagation of an ion acoustic shock [21], and the direct implicit method has been used to simulate ion acoustic fluctuations [22].

The EFPI code in this study uses the PIC code as its ''inner'' microscopic simulator. The global (coarse) variables are first ''lifted'' to a fine scale microscopic representation with which the PIC code is initialized. The PIC code is stepped forward in time, and the results are ''restricted,'' or smoothed, to the coarse representation and saved for each time step. Using a least squares fit, the time derivatives of the coarse variables are estimated at each grid point. Finally, the value of each coarse variable grid point is projected forward with a large time step and the process is repeated.

We find that the Equation Free Projective Integration code, EFREE, reproduces the kinetic code (P3D) quite well. The only differences which do arise are due to physics assumptions made in the lifting algorithm of EFREE, specifically that the ion distribution functions remain maxwellian and that the plasma remains quasi-neutral. Interestingly, there is a Courant condition on the EFREE coarse projection time step based upon the coarse grid and the ion acoustic wave sound speed, even though no explicit macroequations are explicitly written and evolved. We also find that the restriction to the coarse grid is critical for allowing EFPI to be suitable for this test problem. Without the restriction to the coarse grid, fluctuations in the variables make an accurate least squares fit impossible, and the Courant condition requires the coarse time step to be prohibitively small.

Most exciting for this 1D study are the results of the speedup of EFREE over P3D. For the largest system size in this study, EFREE shows a speedup of about 13. This speedup scales linearly with system size. Thus, the speedup of EFREE over P3D will become larger with system size, and is expected to become larger with added dimensions.

2. Ion acoustic wave: theory

This study uses as a test case the ion acoustic wave. We begin with a straightforward fluid analysis of the linear ion acoustic wave. The fluid equations used for the derivation are

$$\frac{\partial n_i}{\partial t} + \nabla \cdot (n_i \mathbf{V}_i) = 0 \tag{1}$$

$$m_i \left(\frac{\partial}{\partial t} + \mathbf{V}_i \cdot \nabla \right) \mathbf{V}_i = -\frac{\nabla P_i}{n_i} + e\mathbf{E} \tag{2}$$

$$0 = -\frac{\nabla P_e}{n_e} - e\mathbf{E} \tag{3}$$

$$\frac{\partial P_i}{\partial t} + \mathbf{V}_i \cdot \nabla P_i + \gamma_i P_i \nabla \cdot \mathbf{V}_i = 0 \tag{4}$$

$$\nabla \cdot \mathbf{E} = 4\pi e(n_i - n_e), \tag{5}$$

where n is density, $\mathbf{V}$ is velocity, P is pressure, and the subscript "i" and "e" refer to positive ions (protons) and electrons. In using these equations we have ignored electron inertia terms (m_e) and used isothermal electrons ($\gamma_e = 1$) because the electron thermal speed is so much faster than the sound speed. We set the electron temperature initially spatially constant, which allows $\nabla P_e = T_e \nabla n_e$ for all time. Linearizing the equations, $\mathbf{f}(\mathbf{x}, t) = \mathbf{f}_0(\mathbf{x}) + \tilde{\mathbf{f}} e^{(i\mathbf{k}\cdot\mathbf{x} - \omega t)}$, and assuming $\mathbf{V}_0 = 0$ yields the following dispersion relation:

$$\omega^2 = \frac{k^2 C_{se}^2}{1 + k^2 \lambda_{\mathrm{De}}^2} + k^2 C_{si}^2, \tag{6}$$

where $C_{se}^2 = T_e/m_i$, $C_{si}^2 = \gamma_i T_i/m_i$, $\lambda_{\mathrm{De}} = C_{se}/\omega_{pi}$. This is the ion acoustic wave including a finite ion temperature and electron Debye corrections. To make sure that ion Landau damping is weak, it is necessary to take $T_e/T_i \gg 1$ [23].

3. Full particle code: P3D

The kinetic simulation code P3D [24,25] is used in this study as both the "inner" microscale simulator for the equation free code EFREE and used as a "correct" simulation for comparison purposes. It is a fully electromagnetic particle-in-cell (PIC) code which is parallelized using MPI for runs on massively parallel computers. The simulations in this study were run on 1 node (16 processors) of an IBM SP. Although the code steps forward the full electromagnetic equations, for the 1D ion acoustic wave used in this study, the magnetic fields play no role. We therefore normalize our equations as follows. Length (L_0) is normalized to the length of the smallest simulation in this study, velocity (V_0) is normalized to $\sqrt{T_0/m_i}$, with $T_e \to T_e/T_0$ and $T_i \to T_i/T_0$. Although B_0 plays no role, it requires a normalization factor for the equations, so we define B_0 such that $eB_0/(m_i c) = V_0/L_0$. The normalized equations are

$$\frac{\partial \mathbf{B}}{\partial t} = -\nabla \times \mathbf{E} \tag{7}$$

$$\frac{\partial \mathbf{E}}{\partial t} = \bar{c}^2 \nabla \times \mathbf{B} - \bar{\omega}_{pi}^2 \mathbf{J} \tag{8}$$

$$\nabla \cdot \mathbf{E} = \bar{\omega}_{pi}^2 (n_i - n_e), \tag{9}$$

where $\bar{c}$ is the normalized speed of light, $\bar{\omega}_{pi}$ is the normalized ion plasma frequency, and $\mathbf{J}$ is the total current calculated by summing the velocities of particles around each grid point. A multigrid relaxation algorithm is

used to correct **E** such that Eq. (9) is satisfied. The **E** and **B** fields are interpolated to the location of each particle, and each particle is stepped forward using:

$$\frac{d\mathbf{V}_\alpha}{dt} = \frac{q_\alpha m_i}{m_\alpha}[\mathbf{E} + \mathbf{V}_\alpha \times \mathbf{B}] \tag{10}$$

$$\frac{d\mathbf{x}_\alpha}{dt} = \mathbf{V}_\alpha, \tag{11}$$

where the α represent electrons or ions and q_α is the sign of the charge for the species.

We initialize both the EFREE and the P3D simulations with the same system. The range of x in the simulations is from 0 to L_x, and $k = 2\pi/L_x$. Setting $\delta n = 0.2$, the initial conditions in code normalized units are

$$\tilde{n}_i \equiv \delta n \sin(kx) \tag{12}$$

$$n_i = 1.0 + \tilde{n}_i \tag{13}$$

$$V_{ix} = V_{\text{shift}} + \frac{\omega}{k}\tilde{n}_i \tag{14}$$

$$P_i = T_{i0}(1 + \gamma_i \tilde{n}_i) \tag{15}$$

$$T_i = \frac{T_{i0}(1 + \gamma_i \tilde{n}_i)}{1 + \tilde{n}_i} \tag{16}$$

$$E_x = -\frac{T_{e0}}{n_i}\frac{\partial \tilde{n}_i}{\partial x} \tag{17}$$

$$n_e = n_i - \frac{1}{\bar{\omega}_{pi}^2}\frac{\partial E_x}{\partial x} \tag{18}$$

$$V_e = V_i \tag{19}$$

ω is the ion acoustic frequency defined in Eq. (6). In code units, $C_{se}^2 = T_{e0}$, $C_{si}^2 = \gamma_i T_{i0}$, $\lambda_{\text{De}}^2 = T_{e0}/\bar{\omega}_{pi}^2$, with $T_{e0} = 1.0$, $T_{i0} = 0.05$, $\bar{\omega}_{pi} = 36$, $\bar{c} = 120$. $m_i/m_e = 1800$. As seen from Eqs. (14) and (19), V_{ix} and V_{ex} are shifted by $V_{\text{shift}} = -1.0$ so that the simulations are performed in a frame basically co-moving with the wave (the phase speed of the wave in the lab frame is ≈ 1.06) [26]. There are 5000 particles per grid cell. It is necessary to take $T_{e0} \gg T_{i0}$ in order to minimize Landau damping. E_x, n_e, and V_{ex} are calculated directly from the full nonlinear equations because they are passive variables in the EFREE code, and Eqs. (17)–(19) define the procedure for their determination in the EFREE code.

The electrons have a very large thermal speed, much larger than the sound speed of the wave. Every electron therefore samples multiple waves over 1 period, leading to significant mixing, so the electrons act isothermally ($\gamma_e = 1$). The ions, however, because their thermal velocity is much less than the sound speed are nearly adiabatic, which in a 1D system corresponds to $\gamma_i = 3$. In the simulations in this study, however, the initial conditions were used setting $\gamma_i = 1$. This leads to a backward propagating ion acoustic wave with $\delta n_i \approx 0.005$, as well as an entropy mode with $\delta n_i \approx 0.017$. Both of those density amplitudes, however, are smaller than the random noise in the n_i due to the finite number of particles per cell, and have little if any discernible effect.

The individual electron and ion particles must be loaded in such a way that they are consistent with the number densities, velocities, and temperatures in the physical system. In order to minimize the initial noise in the system, the particles are given a quiet start [27]: The number of particles needed to generate a given density are loaded randomly around each grid point, which ensures that each Debye sphere has an equal number of electrons and ions. These particles are loaded with a maxwellian distribution in velocity space with a velocity shift consistent with the velocities and temperatures at that grid point.

The sets of simulations used in this study are shown in Table 1.

4. Equation Free Projective Integration: EFREE

Simulating multiscale problems is extremely difficult because of the intimate coupling between the fine scale physics with the coarse grained dynamical behavior. Kinetic simulations include all of the microscale physics,

Table 1
Simulation run sets used for this study

Set #	Type	L_x	n_{xm}	n_{xc}	N_e (range)
1	P3D	1.0	128	–	–
2	EFREE	1.0	128	32	10–20
3	P3D	2.0	256	–	–
4	EFREE	2.0	256	32	10–20
5	P3D	4.0	512	–	–
6	EFREE	4.0	512	32	10–20
7	P3D	8.0	1024	–	–
8	EFREE	8.0	1024	32	10–20
9	EFREE	2.0	256	16	20

P3D is the kinetic PIC code and EFREE is the Equation Free Projective Integration code. L_x is the system length. n_{xm} and n_{xc} are the number of micro and coarse grid points, respectively. N_e is number of micro time steps during each projective integration cycle.

but are too computationally expensive to simulate the full macroscopic system. Macroscopic codes using some fluid closure can simulate global scales, but leave out important microscale physics. The Equation Free Projective Integration method (EFPI) attempts to address these problems by stepping forward data on a coarse representation, but instead of determining the time derivatives of the coarse variables from a set of fluid or other equations, they are estimated on demand by the results of short bursts of an appropriately initialized ensemble of kinetic simulations.

The basic idea of EFPI is that there are two representations of the data. One, a micro kinetic representation in which the system is fully defined down to some fundamental level with very fine spatial and temporal resolution. And two, a coarse representation in which the system is approximated by some smaller number of variables with much coarser spatial and temporal resolution. Translating data back and forth between these two representations is called respectively lifting and restricting: lifting takes data from coarse to micro, and restricting takes data from micro to coarse. In restricting the data, substantial microscale information is lost due to discarded variables and loss of resolution. In lifting the data, interpolation of some kind and assumptions must be made in order to fill in the information which is not included in the coarse representation. Choosing which variables to use in the coarse representation is extremely important, and is driven by our physical knowledge of the system, or through data mining techniques such as diffusion maps [28].

In this test case of EFPI, the kinetic simulator will be P3D, a fully electromagnetic particle-in-cell (PIC) kinetic code. The microrepresentation contains discrete ion and electron particles as well as the electric field. The coarse variables are all moments of the ion (proton) distribution function determined from the discrete ion particles. The code which utilizes EFPI is called EFREE.

Fig. 1 shows the basic projective integration cycle used in this study. At the beginning of the cycle, the coarse representation of the data is known, as shown in Fig. 1a which shows the ion density, n_i versus x. The coarse representation of the data is comprised of "active variables," i.e. those coarse variables which are directly integrated forward in time. This data is then lifted onto a grid with much finer spatial resolution (in this case 16 times more) through a simple linear interpolation. The lifting sequence also must fill in the data needed to initialize P3D which is not directly represented in the coarse representation (called "passive variables"). After the lifting, P3D is initialized using the fine representation, shown in Fig. 1c. Notice the random noise in the kinetic initialization, which is due to the finite number of particles per grid cell. The kinetic code is then stepped forward some N_e number of steps, where the "e" stands for extrapolation, as shown in Fig. 1d and e. This data is then restricted through a simple linear smoothing to give the coarse representation at each time (Fig. 1f and 1g). Finally, in Fig. 1h, for each of the coarse grid points (32 in this case), a least squares fit is performed on the restricted data to determine the time derivative ($\partial n_i/\partial t$ in this case) and that time derivative is used to project the coarse variable forward by a large projection step $\Delta t_p = N_p \Delta t_m$, where Δt_f is the fine scale grid step. The result is shown in Fig. 1i, which shows the coarse data projected forward a time of Δt_p. The whole cycle then repeats.

We emphasize that the two-scale grid structure used in this study is critical for allowing the speedup of the Equation Free Projective Integration algorithm. In this study, we find that without restricting the data to a coarse representation, the level of fluctuations is too high to accurately estimate a time derivative through

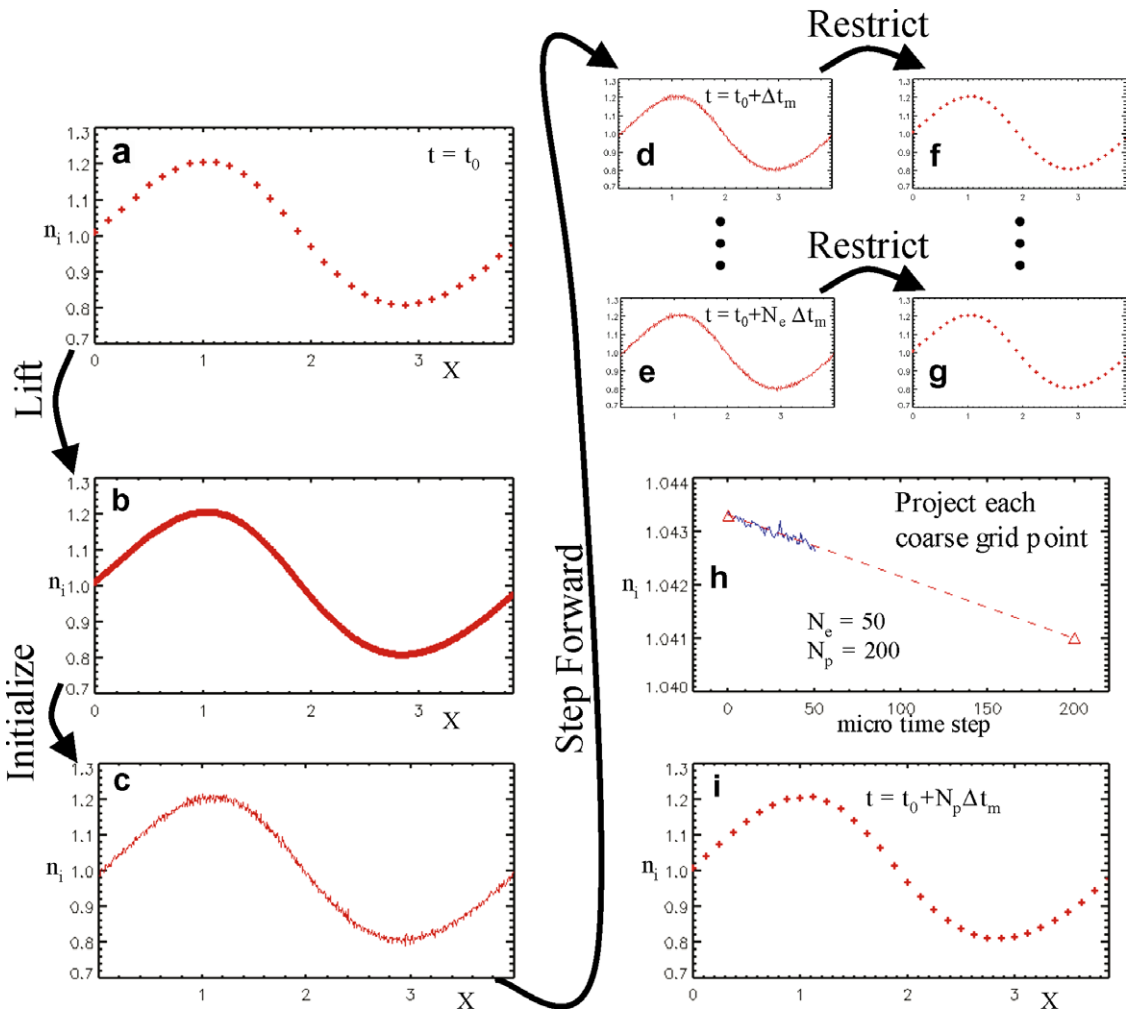

Fig. 1. An overview of the projective integration cycle of EFREE, the Equation Free Projective Integration code using a kinetic particle code (P3D) as its fine scale solver.

fitting. In addition, we find a Courant condition based on the coarse grid and the sound speed, which implies that projectively integrating on a microscopic grid would require a time step that is much too small to be useful for multiscale problems.

We now describe in detail each step of the projective integration cycle.

Coarse representation of data. In this study, the coarse data usually has a total of 32 grid points along x (except for run 9), as can be seen in Table 1. As mentioned above, those variables which are directly projectively integrated forward are called "active" variables. The choice of which variables are active is extremely important, and must include those variables critical for correctly describing the dynamics of the coarse system. For this study, we take n_i, V_{ix}, and P_i as active variables. E_x and n_e are treated as passive quantities and are calculated directly from the active variables.

Lifting and active variables. Lifting requires two important actions: Increasing the resolution of data using linear interpolation; and determining the non-active coarse variables needed to initialize the full particle code.

The linear interpolation is done in successive factors of two. Suppose there are n_{xc} coarse data points for the variable f. The first level of interpolation is

$$\text{for } i = 1, n_{xc} \quad f_{2i}^{(1)} = f_i, \quad f_{2i-1}^{(1)} = 0.5(f_{i-1} + f_i), \tag{20}$$

where (1) represents the first level of interpolation and f_i is the ith grid point of f. Periodic boundary conditions are assumed, so that $f_0 = f_{n_{xc}}$ and $f_{n_{xc}+1} = f_1$. After ℓ iterations, $f^{(\ell)}$ will have $n_{xm} = 2^{\ell} n_{xc}$ grid points.

The next step is to "fill in" the passive variables which are necessary in order to initialize the full particle simulation. It is assumed that both electrons and ions maintain a maxwellian distribution function, so only density, velocity, and pressure are necessary to completely determine the distribution function of each species. The passive variables are determined as follows:

$$E_x = -\frac{T_{e0}}{n_i}\frac{\partial n_i}{\partial x} \tag{21}$$

$$n_e = n_i - \frac{1}{\bar{\omega}_{pi}^2}\frac{\partial E_x}{\partial x} \tag{22}$$

$$V_{ex} = V_{ix} \tag{23}$$

$$T_e = T_{e0} \tag{24}$$

$$T_i = P_i/n_i \tag{25}$$

$$V_{ey} = V_{ez} = V_{iy} = V_{iz} = 0 \tag{26}$$

$$E_y = E_z = 0 \tag{27}$$

$$B_x = B_y = B_z = 0. \tag{28}$$

Note that $P_i = P_{ixx}$, where P_{ixx} is the xx component of the ion pressure tensor. In Eq. (21), it is assumed that $n_i \approx n_e$, which will eventually break down as the wave becomes extremely steep. Before this approximation ceases to be valid, however, the ions in this study become non-maxwellian. Eqs. (21) and (22) could also be iteratively solved to allow quasi-neutrality to be broken during an EFREE run.

Microscopic code initialization. Once all of the necessary microvariables are determined during the lifting process, P3D is initialized.

Microscopic stepping. After it is initialized, the kinetic code is stepped forward N_e steps using a time step Δt_m, where the "e" stands for extrapolation step.

Restricting. After each microscopic time step, the data is restricted onto the coarse grid. In restricting the data, all but the active variables n_i, V_i, and $P_i = P_{ixx}$ are thrown out. The restricting of the active variables is a linear smoothing operation. Suppose that there are n_{xm} micro grid points. The first level of restricting is:

$$\text{for } i = 1, \frac{n_{xm}}{2} \quad f_i^{(1)} = 0.25 f_{2i-1} + 0.5 f_{2i} + 0.25 f_{2i+1} \tag{29}$$

where in this case the (1) represents the first level of restricting. As above, periodic boundary conditions are assumed. f^{ℓ} will have $2^{-\ell} n_{xm}$ grid points. This linear smoothing is repeated until n_{xc} is reached.

Projective integration. At this point, for each active variable f there are N_e data points corresponding to the N_e time steps for each of the n_{xc} grid points. At each grid point, a least squares fit is used to determine the best fit slope in time of the active variable, $\dot{f}$. The variable is then projected forward using:

$$f(t + \Delta t_p) = f(t) + \Delta t_p \dot{f}. \tag{30}$$

Trapezoidal leapfrog. The timestepping shown in Eq. (30) is not exactly what is done for this code. In order to increase the accuracy of the integration forward in time, a trapezoidal leapfrog method is employed to step the active coarse variables forward in time. Each Δt_p time step forward is actually two equation free cycles shown above. The time derivative of a coarse variable $\dot{f}(t)$ is determined through the procedure described above. The full stepping process is

$$f(t+\Delta t_p/2) = \frac{1}{2}[f(t-\Delta t_p) + f(t)] + \Delta t_p \dot{f}(t) \tag{31}$$

$$f(t+\Delta t_p) = f(t) + \Delta t_p \dot{f}(t+\Delta t_p/2). \tag{32}$$

5. Ion acoustic wave: simulation results

Fig. 2 shows the ion density at many different times for a full particle simulation of the ion acoustic wave (run 5 in Table 1). Each successive time is shifted up by a small amount.

The random density fluctuations are quite noticeable. Initially they are quite small owing to the quiet start, but within about 40 micro time steps ($\Delta t \approx 0.0067$) they grow to their asymptotic size. In this study we find that the restriction to the coarse scale is critical for reducing the fluctuations in the active variables to a level that allows an accurate determination of $\partial/\partial t$ from a least squares fit. Even with restriction, however, the net charge $(n_i - n_e)$ and thus the electric field E_x are still too noisy to be usable as active variables. That is why we use Eq. (21) to determine the electric field as a passive variable. Similarly, the high temperature of the electrons leads to large fluctuations in the electron velocity, rendering it unusable in this study as an active variable. More sophisticated fitting schemes such as maximum likelihood estimation could possible overcome these noise issues [29].

In Fig. 2, the wave progressively steepens until dispersive effects from the electron Debye length ($k\lambda_{De} \approx 1$) become important at about $t = 2.67$. From $t = 2.67$ to $t = 3.33$, a localized electrostatic peak in the ion density forms, which leads to a very large bipolar electric field. This localized peak breaks quasi-neutrality and therefore cannot be reproduced with the EFREE lifting algorithm used in this study.

The behavior of other variables in the kinetic simulations as well as the results for EFREE are shown in Fig. 3. At $t = 0$, the P3D and EFREE are very close. Differences are the result of random noise due to the finite number of particles in the simulations. Note that the average initial $V_{ix} = -1.0$ because the simulations are performed in a reference frame moving approximately with the wave velocity. At $t = 1.33$, n_i and V_{ix} both show

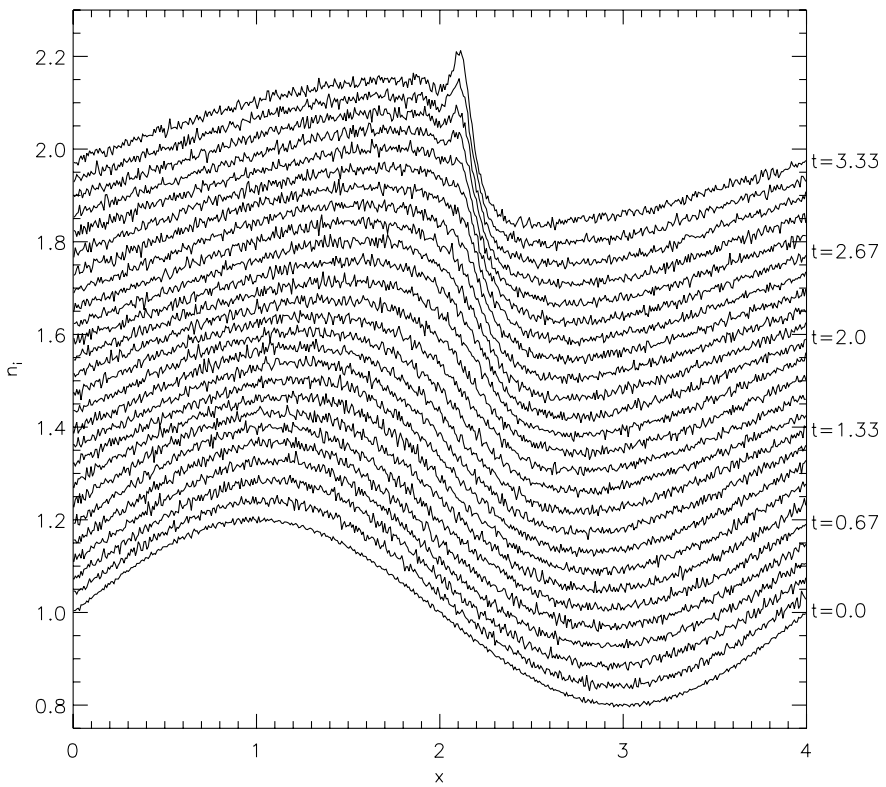

Fig. 2. Ion density versus x for run 5. Each successive time is shifted upwards by $\Delta n_i = 0.04$, and the time between each plot is $\Delta t = 0.133$. The simulation is performed in a frame moving with a velocity $V_{\text{frame}} = 1.0$, which is approximately the wave velocity.

some steepening, but P_{ixx} has increased substantially and is strongly anharmonic compared to n_i and V_{ix}. Comparing P3D and EFREE, n_i and V_{ix} are very similar, but there is already a noticeable difference in P_{ixx}. This difference, as well as the anharmonic shape of P_{ixx} is due to the non-maxwellian distribution function of the ions as will be discussed shortly. At $t = 3.33$, the wave has steepened in P3D with a strongly localized density peak which leads to a large electric field. n_i and V_{ix} as calculated from P3D and EFREE track well but P_{ixx} does not. These differences are due to three sources: First, EFREE assumes quasi-neutrality which is clearly broken when $k\lambda_{De} \approx 1$ at the shock front. Second, the peak in n_i and E_x is only marginally resolved by the EFREE resolution of $\Delta x = 0.03750$. Third, the ion distribution functions in P3D are now strongly non-maxwellian. Despite all of these shortcomings, the propagation speed of EFREE versus P3D matches almost exactly. In addition, these differences are due to an incomplete representation of the system at coarse scales in EFREE, not to a numerical problem, so including the missing physics in EFREE is likely to reduce the differences.

The evolution of the ion distribution function, f_i, into its non-maxwellian state can be seen in Fig. 4. On the left hand side are grayscale (color online) plots of $\log_{10} f_i$ with contours of total energy, E_{tot}. $E_{tot} = mV_{ix}^2/2 + e\phi$, where $E_x = -\nabla\phi$ and V_{ix} has been shifted into a frame moving with the wave. At $t = 0$, the distribution func-

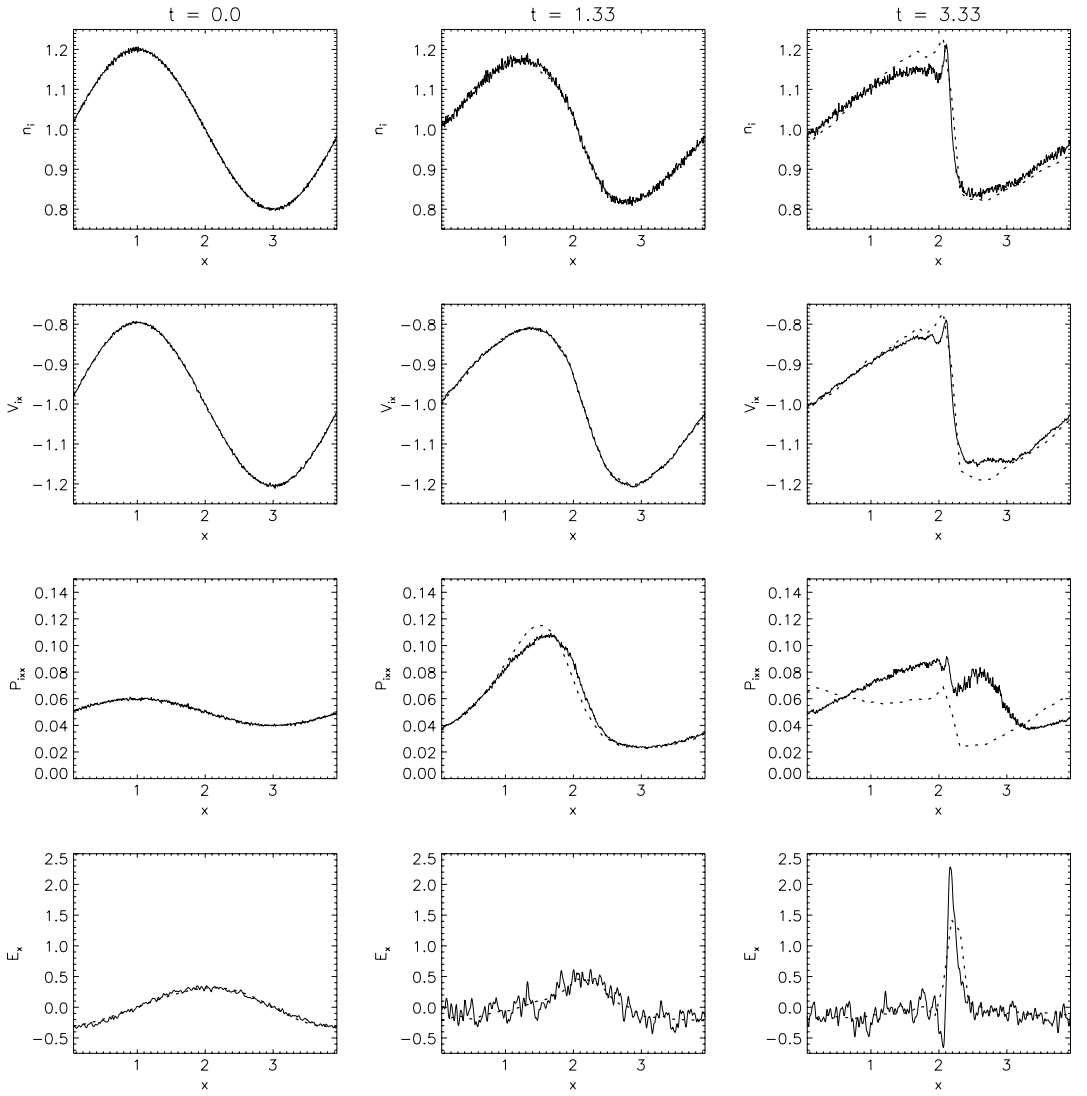

Fig. 3. Full particle results (solid) and EFREE results (dashed) for the ion acoustic wave (runs 5 and 6 with $N_e = 20$. The three active EFREE variables (n_i, V_{ix}, and P_{ixx}) as well as E_x are shown. The times shown are (left) $t = 0.0$, (middle) $t = 1.33$, and (right) $t = 3.33$.

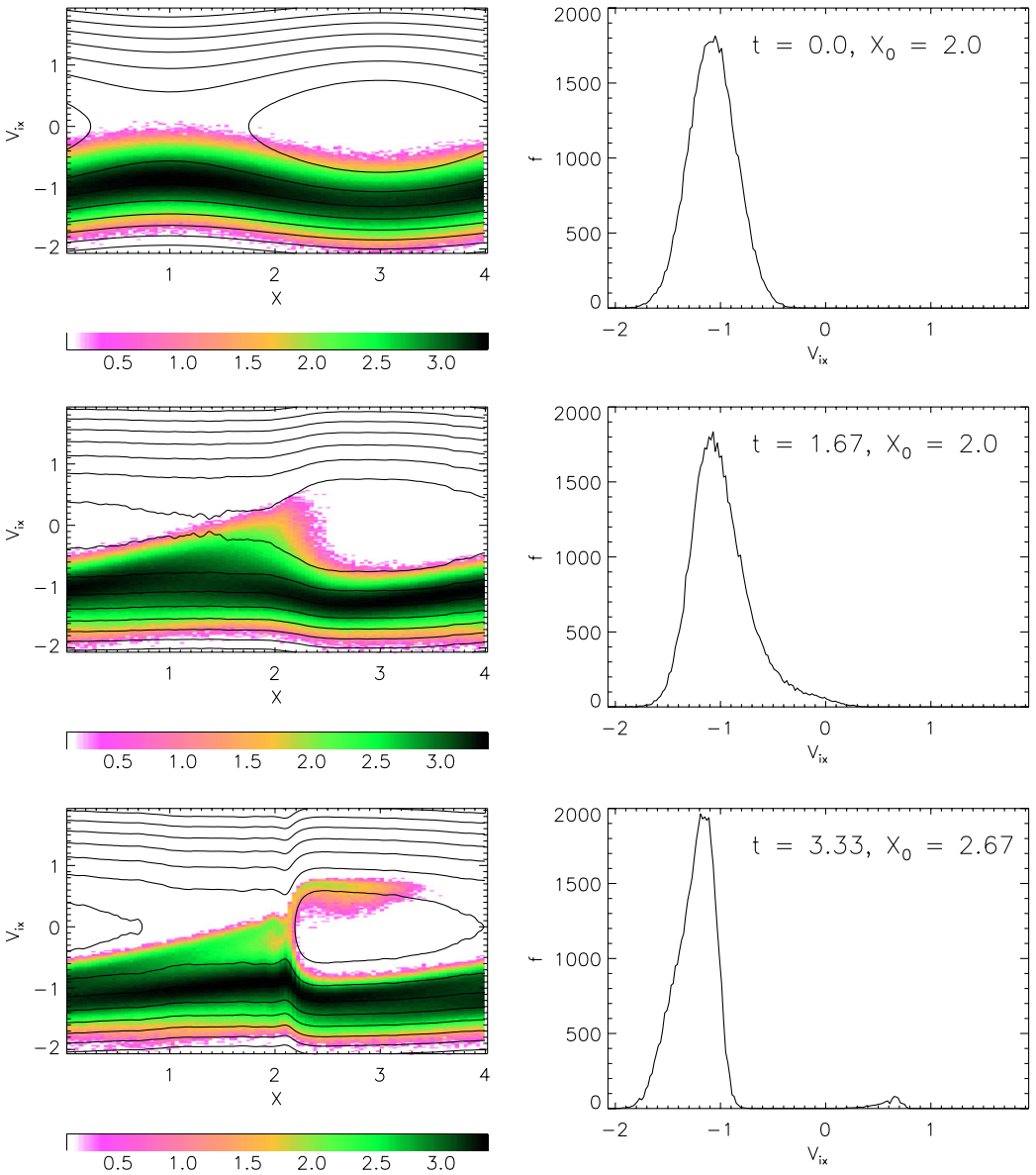

Fig. 4. Unnormalized ion probability distribution functions, $f_i(x, v)$, at three different times for a P3D run (run 5). Left plots: grayscale (color online) of $\log_{10} f_i$, with total energy contours. Right plots: Cuts of f_i along V_{ix} at a given $x = x_0$. Top: $t = 0.0$, Middle: $t = 1.67$, Bottom: $t = 3.33$.

tion is a shifted maxwellian with a velocity shift dependent on x. Note that for $x > 2$ the low speed tail of the maxwellian lies on trapped energy contours. At $t = 1.67$ in the vicinity of $x \approx 2$, this low speed tail has started to reflect. By $t = 3.33$, the reflected particles are unmistakable and the distribution function is double peaked.

6. Scaling properties

Although the good agreement for the propagation and steepening shown in the previous section is very promising, it must be accompanied by a speedup in the runtime of EFREE over P3D in order for EFREE to be a viable multiscale simulation code. The majority of computational time used to run EFREE is used during the stepping of the microscopic kinetic simulations on the micro grid. The time to lift, restrict, deter-

mine the time derivative of the active coarse variables, and project them forward in time is relatively small in comparison. Thus, the speedup depends on keeping the number of kinetic micro time steps (N_e) during each projective integration cycle small and making the projective integration time step (Δt_p) as large as possible. Most important is how these quantities change as the system becomes larger.

An important question determining the usability of EFREE are the timescales which must be resolved for stable stepping. In the P3D ion acoustic wave, the light wave, electron plasma wave, and electron thermal velocity all place stringent requirements on the particle time step, requiring $\Delta t_m = 0.000167$ for good energy conservation. If EFREE is required to resolve any of these microscale times with the coarse time step Δt_p, it will not be a viable multiscale code. For this set of simulations, however, we find the stability condition $\Delta t_p \lesssim \Delta x_c/(2c_s)$, a Courant condition based on the macroscopic sound wave speed. This is heartening not only because c_s is a macroscale effect, but also as expected EFREE is limited by a physical effect, even though there are no explicit equations at the macroscopic scale. This is seen in Fig. 5, which is the maximum stable time step versus grid scale. The approximate slope of the points is about 1/2, consistent with the Courant condition given above. This Courant condition shows why restricting the data before projecting it forward is critical for making EFPI viable. Reducing Δt_p to a Courant condition based on the microscopic grid scale would make EFREE too computationally expensive to be used to study multiscale problems.

Determining the minimum number of time steps N_e necessary for stability and good accuracy is more challenging. We define an error function ϵ as

$$\epsilon^2 = \frac{\sum_{j=1}^{n_{xc}} (n_j^{\mathrm{EFREE}} - n_j^{\mathrm{P3D}})^2}{\sum_{j=1}^{n_{xc}} [(n_j^{\mathrm{EFREE}})^2 + (n_j^{\mathrm{P3D}})^2]}, \tag{33}$$

where n_j^{EFREE} is the jth coarse grid cell in the EFREE output and n_j^{P3D} is the jth coarse grid cell in the P3D output. For this study, we present only the error results for n_i, but we also examined the results using V_{ix} and the conclusions were the same. The coarse representation of P3D data is done by restricting the microscale data output after the P3D simulation has finished. The numerator in Eq. (33) is a measure of the total difference between P3D and EFREE, and the denominator is a normalization factor. Fig. 6a shows the growth of error versus time for six different values of N_e in run 6. From $t = 0$ to $t = 0.5$ the error remains quite low for the cases with larger N_e. At later times, the error grows quickly because of the non-maxwellian assumptions in EFREE. Most interesting, however, is that at early times, $N_e = [16 - 20]$ are indistinguishable whereas for $N_e \leqslant 14$ there is clearly a diverging error. This analysis allows us to determine the smallest N_e possible to retain the highest accuracy. In this case, $N_{\mathrm{emin}\approx 16}$.

Performing this analysis on 4 different system sizes (each with 32 coarse grid points) gives the results shown in Fig. 6b. Quite surprisingly, N_{emin} remains roughly constant as the system size is increased. The effect this has on the runtime of EFREE is dramatic. As L_x is doubled in this set of simulations, the time it takes to run the kinetic microstepper is doubled because the number of microscale grid points and the number of particles doubles. However, the Courant conditions gives $\Delta t_p \sim L_x/(n_{xc}c_{s0})$, with $n_{xc} = 32$. This means that Δt_p doubles if L_x doubles, so the increased computation time used during the microscopic simulations is offset by the larger

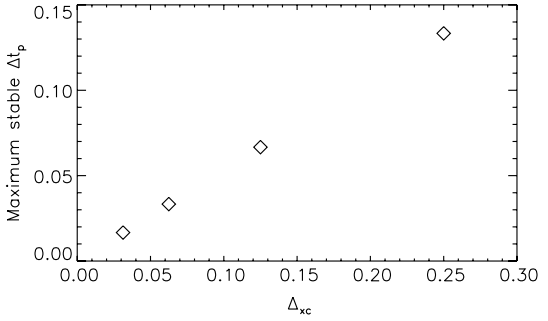

Fig. 5. Largest projective integration time step Δt_p possible versus coarse grid scale Δx_c. These results are for runs 2,4,6,8,9 in Table 1 with $N_e = 20$.

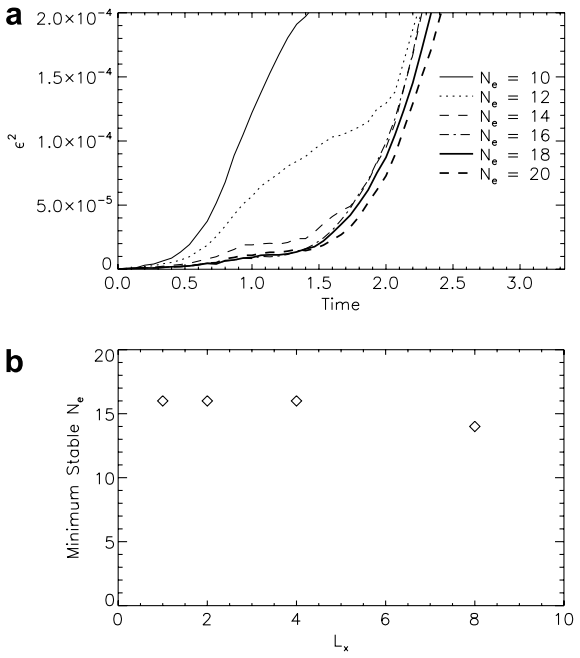

Fig. 6. (a) The error function (ϵ^2) versus time for various N_e of run 6 in Table 1. (b) Minimum N_e necessary to reach asymptotic error versus system size L_x. The accuracy of minimum N_e is about ± 2.

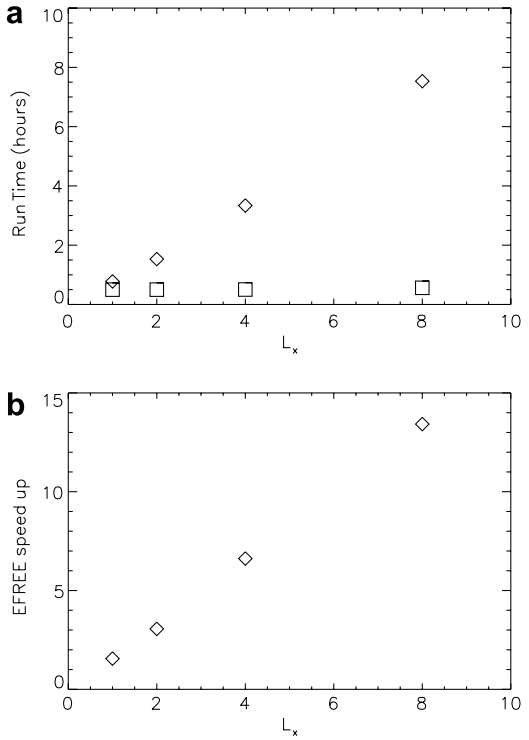

Fig. 7. (a) Time to run one $t_0 = L_0/C_{s0}$ versus system size L_x for runs 1–8 in Table 1 with $N_e = 20$. The P3D runs are shown as diamonds, and the EFREE runs are shown as squares. All simulations were performed on 16 processor of an IBM SP II. Note that the normalization length L_0 is chosen so that the smallest system has a length of 1.0. (b) Speedup factor between identical EFREE and P3D runs.

coarse time step. As seen in Fig. 7a, the time for EFREE to run one normalized time unit ($t_0 = L_0/c_{s0}$) remains constant as the L_x is increased. Note that L_0 is chosen so that the smallest simulation has a length of 1.0 and that all simulations are run on 16 processors of an IBM SP II. For P3D, on the other hand, the run time increases linearly with L_x, giving a speedup factor for EFREE that scales linearly with L_x, as shown in Fig. 7b. For a 1D system, this is quite a large speedup. For the largest system with $L_x = 8$, the speedup is 13×, and is expected to become even larger for a 2D or 3D system.

This linear speedup and independence of N_{emin} from L_x is quite surprising. One would expect N_{emin} to be dependent on the accuracy of the projective integration. The signal to noise ratio of the least squares fit used to determine the time derivative in EFREE is equal to $\xi \sim \sigma_f/M_t$, where σ_f is the error in the least squares fit and M_t is the time derivative. The random noise associated with fluctuations in the number of particles is expected to scale as $N_{\text{ppg}}^{-1/2}$, where N_{ppg} is the number of particles per coarse grid. From the derivation of least square, $\sigma_f \sim (N_{\text{ppg}}N_{\text{emin}})^{-1/2} \sim (L_xN_{\text{emin}})^{-1/2}$. With $M_t \sim L_x^{-1}$, this gives $\xi \sim \sqrt{L_x/N_{\text{emin}}}$. Requiring ξ be greater than some threshold value implies $N_{\text{emin}} \sim L_x$, which contradicts the computational results. This simple argument, however, assumes that there is no feedback mechanism to minimize perturbations as they form. A grid scale perturbation in the density will decrease in magnitude due to dispersion during sound wave propagation, which has been verified using EFREE.

To further demonstrate that the random noise due to the number of particles per grid is not controlling N_{emin} for this study, we have performed the error analysis used in Fig. 6a on EFREE runs with the same parameters as run 6 but with $N_{\text{ppg}} = 1250$ and 20,000. Although ϵ is larger for smaller values of N_{ppg}, the value of N_e at which ϵ asymptotes does not change with N_{ppg}. N_{emin} is independent of N_{ppg}, which implies that error associated with the finite number of particles per cell is not controlling N_{emin}.

7. Conclusions

In this study we sought to determine if Equation Free Projective Integration (EFPI) has the potential to be a viable method for simulating plasmas using kinetic particle-in-cell (PIC) codes as the microstepper. Because EFPI is such a novel technique, having no dynamical equations at the course scales, we applied it first to the well known problem of the propagation and steepening of an ion acoustic wave. We stress that this is not a multiscale system, and our ultimate goal for EFPI is not to study the ion acoustic mode. Our goal for this study is to make an initial determination if EFPI can successfully simulate a simple plasma system like the ion acoustic wave. The main findings are

- Equation Free Projective Integration (EFPI) with a kinetic PIC micro-simulation can accurately simulate the propagation and steepening of an ion acoustic wave.
- The differences which do arise between the EFPI and fully kinetic simulation (P3D) are due to the physics discarded in the lifting to the coarse representation: the assumption of maxwellian ions and quasi-neutrality. Generalizing the course representation to include non-maxwellian ions and Debye length structures should minimize these differences.
- The coarse time step is not dependent on the micro grid scale, but instead is determined with a Courant condition based on the ion acoustic wave speed and the course grid scale. In this study, this leads to a speedup of EFREE over the kinetic simulation (P3D) which scales linearly with system size, being 13 times faster for the largest simulation performed.

From these findings we conclude that EFPI has the potential to be a viable candidate for simulating multiscale plasma problems. We wish to emphasize, however, that the propagation and steepening on an ion acoustic wave is not a multiscale problem. The efficacy of EFPI for multiscale plasma dynamics still needs to be demonstrated.

One should not draw the conclusion from this study that EFPI is more effective at simulating the ion acoustic wave than more conventional techniques such as implicit Particle-in-Cell (PIC) [15,18] or "Multiscale" PIC [21]. The time step in implicit PIC, for example, is not limited by physics which is not resolved in the simulation (often plasma waves and Debye scales). The ultimate goal of studying EFPI is not to simulate basic ion acoustic phenomena more effectively, however. Simulating the ion acoustic wave is simply a first pass

at determining the strengths and weaknesses of using EFPI on plasma systems. If successful, EFPI will be used to simulate physics phenomena that defy simulation through conventional means. Reconnection is one such example, and a particular reconnection question which may be well suited to EFPI is highlighted below. The real strength of EFPI is that it has the potential to include the coarse scale effects of microscale physics, while having a coarse time step not limited by such microscale physics.

The application of EFPI used in this paper is only one subset of possible EFPI algorithms. The method is quite general, and allows any micro-stepping algorithm, whether it be explicit kinetic PIC, implicit PIC, Vlasov, hybrid, two-fluid, or even MHD. Or course, the kinetic stepper must be chosen carefully to include those physical aspects which are deemed ''important'' for the problem being addressed.

Before attempting to apply EFPI to a truly multiscale problem, there are several issues that will probably need to be addressed. One, it should be demonstrated that EFPI can work effectively on more general non-maxwellian distribution functions. We are currently studying a method of representing the distributions using a wavelet analysis. Two, the issue of random fluctuations due to PIC codes must be addressed. This issue will probably be most important in problems with active electron variables, for the higher electron thermal velocity will lead to larger fluctuations. If the fluctuations levels are too problematic for PIC codes, it may be necessary to use a Vlasov solver to implement EFPI. Using an implicit PIC code as the microstepper could also combat the problems with fluctuations by simply removing the fast timescale plasma waves from the system if they are deemed to be unimportant for a given problem. Three, a better understanding is needed of the numerical accuracy and stability of EFPI. Although the Courant condition on the coarse time step seems straightforward, the minimum number of micro time steps needed during each projective integration cycle (N_{emin}) is not well understood. Numerical analysis is hindered by the fact that there are no equations that govern the coarse scales.

Ultimately, we hope to apply EFPI to multiscale phenomenon which defy simulation through ordinary means (including implicit techniques). It is clear that EFPI will not be able to simulate these systems while still including all small timescales and length scales at the coarse level. The key is determining which physics is important at the coarse level. This physics will determine both the coarse representation of the system and the lifting method. Not all multiscale problems will be solvable with EFPI. It is only useful for those problems which have a separation of scales between the micro and macroscales, i.e. which have a macro solution on a slow manifold.

In terms of magnetic reconnection, one physics problem which may have adequate separation of scales to allow the use of the EFPI method is the following: Can anomalous resistivity due to electron turbulence play a mediating role in reconnection? In 3D kinetic PIC simulations of reconnection with a modest guide field, it has been found that the current sheet near the x-line goes Buneman unstable and generates turbulence which scatters electrons and causes anomalous resistivity [30]. It is not clear, however, if this anomalous resistivity plays any role in determining the reconnection rate or simply facilitates the change in topology required for reconnection to take place. Determining the role of anomalous resistivity will require large-scale 3D simulations which include electron kinetic physics. EFPI may be ideally suited for this task because of the large separation of time scales between that of the high frequency turbulence and that associated with the global reconnection geometry. The microscopic simulator will resolve all of the turbulence causing an average electron drag. If simulations of EFPI are successful, this electron drag will self consistently manifest itself at the coarse scales as an anomalous resistivity. Implicit particle simulation techniques [15,18] allow large time steps relative to electron timescales, but would completely miss the dynamics of the turbulence if such time steps were used. Therefore, implicit PIC codes are only marginally superior to a normal PIC code in addressing the problem of anomalous resistivity in large-scale reconnecting systems. The development of novel algorithms to address such problems remains an open scientific challenge.

Acknowledgements

The authors wish to thank I. Kevrekidis, S. Cowley, P. Guzdar, and F. Waelbroeck for enlightening discussions. This work was supported in part by the DOE Center for Multiscale Plasma Dynamics at the University of Maryland.

References

[1] K. Theodoropoulos, Y.-H. Qian, I.G. Kevrekidis, Coarse stability and bifurcation analysis using timesteppers: a reaction diffusion example, Proc. Natl. Acad. Sci. 97 (2000) 9840.
[2] C.W. Gear, I.G. Kevrekidis, C. Theodoropoulos, Coarse integration/bifurcation analysis via microscopic simulators: micro-Galerkin methods, Comp. Chem. Engng. 26 (2002) 941.
[3] C.W. Gear, I.G. Kevrekidis, Projective methods for stiff differential equations: problems with gaps in their eigenvalue spectrum, SIAM J. Sci. Comput. 24 (2003) 1091.
[4] C.W. Gear, J. Li, I.G. Kevrekidis, The gaptooth method in particle simulations, Phys. Lett. A 316 (2003) 190.
[5] I.G. Kevrekidis, C.W. Gear, J.M. Hyman, P.G. Kevrekidis, O. Runborg, C. Theodoropoulos, Equation-free multiscale computation: enabling microscopic simulators to perform system-level talks. <arXiv:physics/0209043>.
[6] V.B. Shenoy, R. Miller, E.B. Tadmor, D. Rodney, R. Phillips, M. Ortiz, An adaptive finite element approach to atomic-scale mechanics – the quasicontinuum method, J. Mech. Phys. Solids 47 (3) (1999) 611.
[7] T. Shardlow, A.M. Stuart, A perturbation theory for ergodic Markov chains and application to numerical approximations, SIAM J. Numer. Anal. 37 (4) (2000) 112.
[8] A. Chorin, O. Hald, R. Kupferman, Optimal prediction and the Mori-Zwanzig representation of irreversible processes, Proc. Natl. Acad. Sci. 97 (2000) 2968.
[9] K. Xu, A gas-kinetic BGK scheme for the Navier–Stokes equations and its connection with artificial dissipation and Godunov method, J. Comput. Phys. 171 (1) (2001) 289.
[10] H. Karimabadi, J. Driscoll, Y.A. Omelchenko, N. Omidi, A new asynchronous methodology for modeling of physical systems: breaking the curse of courant condition, J. Comput. Phys. 205 (2005) 755.
[11] X. Yue, W. E, Numerical methods for multiscale transport equations and application to two-phase porous media flow, J. Comput. Phys. 210 (2005) 656.
[12] J. Denavit, Time-filtering particle simulations with $\omega_{pe}\Delta t \gg 1$, J. Comput. Phys. 42 (2) (1981) 337.
[13] R.J. Mason, Implicit moment particle simulation of plasmas, J. Comput. Phys. 41 (2) (1981) 233.
[14] J.U. Backbill, D.W. Forslund, An implicit method for electromagnetic plasma simulation in two dimensions, J. Comput. Phys. 46 (1982) 271.
[15] J.U. Brackbill, D.W. Forslund, Simulation of low-frequency electromagnetic phenomena in plasmas, in: J.U. Brackbill, B.I. Cohen (Eds.), Multiple Time Scales, Academic Press, Inc., 1985, p. 272, Chapter 9.
[16] A. Friedman, A.B. Langdon, B.I. Cohen, A direct method for implicit particle-in-cell simulation, Comments Plasma Phys. Controlled Fusion 6 (1981) 225.
[17] B.I. Cohen, A.B. Langdon, A. Friedman, Implicit time integration for plasma simulation, J. Comput. Phys. 46 (1) (1982) 15.
[18] A.B. Langdon, D.C. Barnes, Chapter 11: Direct implicit plasma simulation, in: J.U. Brackbill, B.I. Cohen (Eds.), Multiple Time Scales, Academic Press, Inc., 1985, p. 336.
[19] D.W. Hewett, A.B. Langdon, Electromagnetic direct implicit plasma simulation, J. Comput. Phys. 72 (1) (1987) 121.
[20] A. Friedman, S.E. Parker, S.L. Ray, C.K. Birdsall, Multi-scale particle-in-cell plasma simulation, J. Comput. Phys. 96 (1) (1991) 54.
[21] S.E. Parker, A. Friedman, S.L. Ray, C.K. Birdsall, Bounded multi-scale plasma simulation: application to sheath problems, J. Comput. Phys. 107 (1993) 388–402.
[22] D.C. Barnes, T. Kamimura, J.N. Leboeuf, T. Tajima, Implicit particle simulation of magnetized plasmas, J. Comput. Phys. 52 (3) (1983) 480.
[23] N.A. Krall, A.W. Trivelpiece, Principles of Plasma Physics, San Francisco Press, Inc., San Francisco, CA, 1986.
[24] M.A. Shay, J.F. Drake, B.N. Rogers, R.E. Denton, Alfvénic collisionless reconnection and the Hall term, J. Geophys. Res. 106 (2001) 3751.
[25] A. Zeiler, D. Biskamp, J.F. Drake, B.N. Rogers, M.A. Shay, M. Scholer, Three-dimensional particle simulations of collisionless magnetic reconnection, J. Geophys. Res. 107 (2002) 1230, doi:10.1029/2001JA000287.
[26] M.E. Kavousanakis, R. Erban, A.G. Boudouvis, C.W. Gear, I.G. Kevrekidis, Projective and coarse projective integration for problems with continuous symmetries, J. Comput. Phys., in press. Also at <math/06081222 at arXiv.org>.
[27] J.M. Dawson, Particle simulation of plasmas, Rev. Mod. Phys. 55 (1983) 403–447.
[28] B. Nadler, S. Lafon, R.C. Coifman, I.G. Kevrekidis, Diffusion maps, spectral clustering and the reaction coordinates of dynamical systems, Appl. Comp. Harm. Anal., in press. Also at <arXiv.org:math/0503445>.
[29] Y. Aït-Sahalia, Maximum likelihood estimation of discretely sampled diffusions: a closed form approximation approach, Econometrica 70 (1) (2002) 223.
[30] J.F. Drake, M. Swisdak, M.A. Shay, B.N. Rogers, A. Zeiler, C. Cattell, Formation of electron holes and particle energization during magnetic reconnection, Science 299 (2003) 873.